CRYSTAL GROWTH & DESIGN

Article

pubs.acs.org/crystal

Characteristics of Strain-Induced $In_xGa_{1-x}As$ Nanowires Grown on Si(111) Substrates

Jae Cheol Shin,[†,‡] Kyoung Jin Choi,[*,§] Do Yang Kim,[⊥] Won Jun Choi,[⊥] and Xiuling Li[*,†]

[†]Department of Electrical and Computer Engineering, University of Illinois, Urbana, Illinois 61801, United States

[‡]Photonic-Energy Center, Korea Photonics Technology and Institute, Gwangju 550-779, Korea

[§]School of Mechanical and Advanced Materials Engineering, Ulsan National Institute of Science & Technology (UNIST), Ulsan 689-805, Korea

[⊥]Nano-Photonics Center, Korea Institute of Science and Technology, Seoul 136-791, Korea

Supporting Information

ABSTRACT: Large strain-energy arising from lattice mismatch allows one-dimensional heteroepitaxial growth of $In_xGa_{1-x}As$ on silicon substrates without any catalyst or pattern assistance. In this paper, we show that in contrast to nanowires (NWs) grown by metal-catalyzed vapor−liquid−solid mechanism, strain-induced $In_xGa_{1-x}As$ NWs have several unique morphological features including no tapering, slight bending, and composition-dependent NW height saturation. Although small fluctuation exists, no systematic composition variations are observed over the entire $In_xGa_{1-x}As$ NW length within the resolution of the energy-dispersive X-ray spectroscopy analysis.

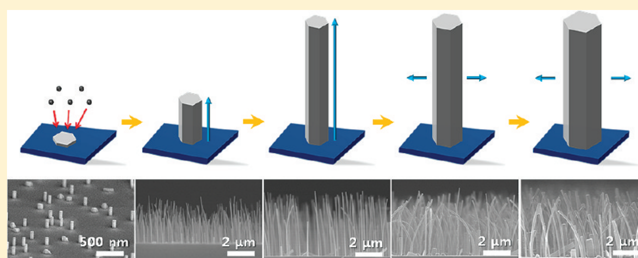

INTRODUCTION

Bandgap engineering of semiconductors is essential to enhance the functionality of the optoelectronic devices.[1] For example, bandgap-engineered $In_xGa_{1-x}As$ can cover the entire near-infrared (NIR) wavelength by adjusting the indium (In) composition.[2] For the growth of heteroepitaxial thin films on substrates, however, enormous strain energy accumulates in thin films resulting from differences in crystal lattice parameters, thermal expansion behavior, etc.[3,4] Therefore, once a certain critical thickness is exceeded, strain relaxation proceeds by formation of misfit or threading dislocations.[5] Thus, it is very challenging to grow bandgap-engineered epitaxial thin films with a wide composition modulation on the same substrate such as $In_xGa_{1-x}As$ on silicon (Si).[6] One-dimensional (1-D) heteroepitaxy on the other hand can accommodate mismatch strain through lateral strain relaxation, allowing NWs epitaxially grown on substrates with as much as 46% lattice mismatch.[7,8] Epitaxial $In_xGa_{1-x}As$ NWs can be synthesized using a variety of methods such as selective-area epitaxy (SAE) or vapor−liquid−solid (VLS) methods.[9−13] However, the former is a time-consuming process due to the preparation of the e-beam lithography pattern,[9] and the latter has the tendency to incorporate metal in the NWs, which could induce deep levels in the bandgap and degrade the device performance.[14] Moreover, the In composition of VLS-grown ternary $In_xGa_{1-x}As$ NW gradually varies along the NW due to the difference of group III and V adatom diffusion lengths; thus the control of energy bandgaps is unfeasible.[12]

We have recently demonstrated catalyst-free, self-assembled heteroepitaxial growth of the $In_xGa_{1-x}As$ NW array on Si substrates over almost the entire composition range by metal−organic chemical vapor deposition (MOCVD), as well as solar cells consisting of $In_xGa_{1-x}As$ NWs on Si substrates.[15] In this paper, we analyze the structural characteristics of the catalyst-free $In_xGa_{1-x}As$ NWs in detail, aiming to shine light on the catalyst-free 1-D growth mechanism. In-rich $In_xGa_{1-x}As$ (x > 0.65) NWs has been chosen for the characterization of the structural properties. The In-rich $In_xGa_{1-x}As$ NWs on Si substrate is highly desirable because its bandgap energy lies below 0.7 eV, which continuously extends the absorption of solar spectrum on Si platform, thus enabling Si-based monolithic tandem solar cells.

EXPERIMENTAL SECTION

Metal−organic chemical vapor deposition (MOCVD) with horizontal reactor was used to grow the $In_xGa_{1-x}As$ NW array on Si. Prior to the growth, a p-type Si(111) wafer (ρ = 0.15−0.25 Ω·cm) was dipped in buffered oxide etch (BOE, Transene Inc.) for 10 min to remove native oxide on the surface. After that, the wafer was rinsed in deionized (DI) water, dried with N_2 gun, and loaded into the MOCVD chamber without delay. The reactor was immediately pumped down to 100 mbar of chamber pressure then heated to the growth temperature (i.e., 560−590 °C) under 15 L/min of hydrogen (H_2) flow. After short stabilization time, trimethylindium [$(CH_3)_3In$, TMIn], trimethylgal-

Received: February 13, 2012
Revised: April 18, 2012
Published: April 23, 2012

ACS Publications © 2012 American Chemical Society

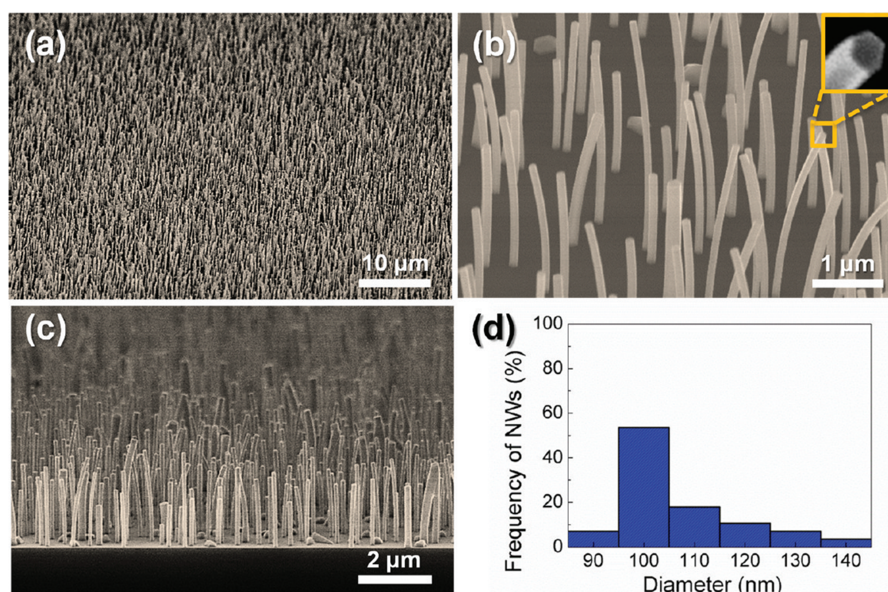

Figure 1. SEM images of $In_xGa_{1-x}As$ NW array with different magnifications and angles. Panels a and b are 45° and panel c is 80° tilted view. Inset in panel b is a high-magnification image showing the hexagonal top of the NW. Panel d is the histogram of NW diameters in a representative area of 25 μm^2.

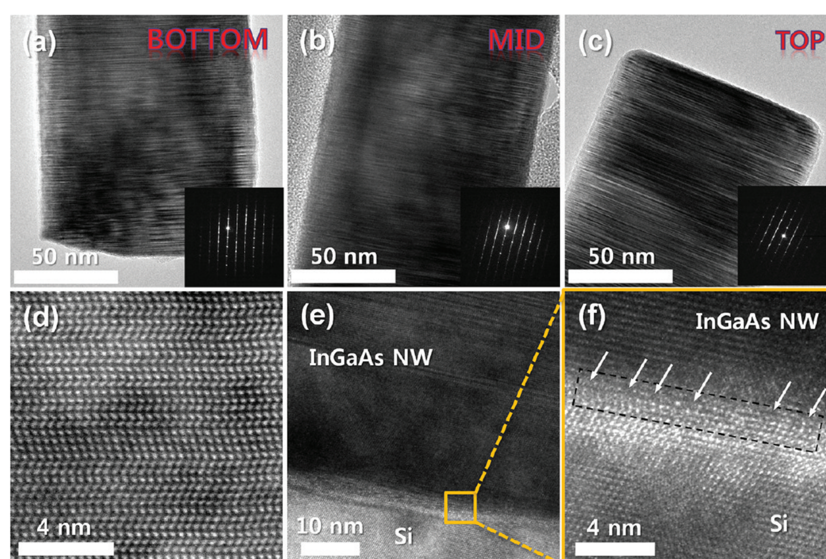

Figure 2. Electron microscopy characterization of an $In_xGa_{1-x}As$ NW grown on Si(111). (a−c) TEM images of the NW along the axial direction (bottom, middle, and top) and corresponding electron diffraction patterns (inset). (d) HR-TEM image of the NW showing the intermixing of WZ and ZB phases and stacking faults. (e, f) Cross-sectional TEM images taken at the interface between $In_xGa_{1-x}As$ NW and Si. Arrows in f indicate misfit dislocations.

lium [$(CH_3)_3Ga$, TMGa], and arsine (AsH_3) were simultaneously flowed into the reactor. At the end of NW growth, TMIn and TMGa were shut down but AsH_3 was maintained until the reactor was cooled to 270 °C. The morphology of $In_xGa_{1-x}As$ NWs was characterized by scanning electron microscopy (SEM, Hitachi-S4800). The structural properties of NWs were investigated by transmission electron microscopy (TEM, Titan 80−300, FEI inc.). Sample for the cross-sectional TEM was prepared using a focused ion beam (FIB). A thick platinum layer was deposited on the sample to protect the surface during the ion milling process. The compositional variation along the NWs was measured using energy-dispersive X-ray spectroscopy (EDX) equipped in the TEM machine. The X-ray spot size for EDX analysis was ~0.1 nm. The In composition (x) of the $In_xGa_{1-x}As$ NW was calculated from the atomic ratio of EDX spectra with an accuracy of error range better than 3%.

■ RESULTS AND DISCUSSION

Figure 1a−c shows the SEM images of $In_xGa_{1-x}As$ NW array grown on a Si(111) substrate. The nominal composition of the NWs is $In_{0.65}Ga_{0.35}As$, based on the In and Ga molar ratio supplied in the gas phase. The vertically aligned NWs were grown on one half of 2 in. Si wafer and found to be mostly uniformly distributed except for the edge areas. The cross-section of the nanowire is hexagonal (inset in Figure 1b) corresponding to the hexagonal lattice of Si(111) surface. As seen in Figure 1b, some of the $In_xGa_{1-x}As$ NWs have slight curvature along the axial direction with longer NWs being more curved. The binary InAs NW, in contrast, is completely vertical along the (111) direction without any bending, as confirmed by

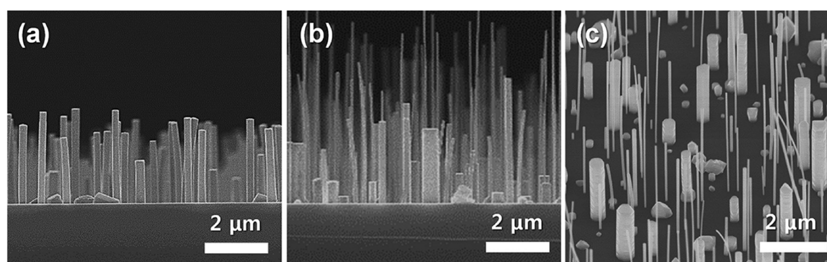

Figure 3. SEM images for $In_xGa_{1-x}As$ NW array: (a) NWs grown for 20 min with In molar ratio [TMIn/(TMGa+TMIn)] of 0.2; (b) NWs grown for 10 min with In molar ratio of 0.2 first, then the ratio changed to 0.65 and NWs grown for another 10 min; (c) 45° tilted SEM image for NWs shown in panel b.

previous study.[15,16] The NW bending phenomenon can be understood from the local inhomogeneity of group III composition producing nonuniform strain across the NWs. However, the composition inhomogeneity in ternary NWs occurs only intermittently for a few monolayers,[15] and no systematic trend in composition variation is observed, which will be discussed with the EDX results below. Figure 1d shows the histogram of the NW diameters over an area of 25 μm^2, which vary in the range of 80 and 150 nm and peak at ∼100 nm. Relatively uniform NWs are distributed over the large area. The density of the NW array is estimated to be >1 × 10^8 cm^{-2} without any pattern or catalyst assistance. In practical applications, a high-density NW array is very important in order to generate enough photons or photocurrents for optoelectronic devices.

Electron microscopy characterization has been performed to analyze the structural properties of the $In_xGa_{1-x}As$ NWs. Figure 2a−c shows TEM images and selective area electron diffraction (SAED) patterns of the $In_xGa_{1-x}As$ NW (nominal In% is 0.65) measured at different NW positions (i.e., bottom, middle, and top). The diameter of NW is very uniform along the NW height, which is in stark contrast to the ternary $In_xGa_{1-x}As$ NWs grown via VLS including self-catalyzed methods using Ga or In droplets.[12,17] SAED patterns in insets indicate that the crystal structure has stacking faults and twin planes along the (111) direction.[18] HR-TEM in Figure 2d clearly shows the mixture of zinc-blende (ZB) and wurtzite (WZ) structures alternating every few monolayers with stacking faults. The cross-sectional TEM images at the interface between Si and $In_xGa_{1-x}As$ NW are shown in Figure 2e,f. The atomically abrupt heteroepitaxial interface between $In_xGa_{1-x}As$ NW and Si can be seen. The NW has ordered ZB structure near the interface but shows mixed crystal structures and stacking faults as the NW grows. The diameter of the $In_xGa_{1-x}As$ NWs is far beyond the critical diameter where misfit dislocations are created.[19] Thus, existence of enormous lattice-mismatch strain (i.e., >9%) generates sporadic misfit dislocations at the interface, which are marked by arrows in Figure 2f. In general, increase of misfit dislocations at the heterojunction yields a threading dislocation, which acts as nonradiative recombination center for optoelectronic devices. However, in this case, threading dislocations or antiphase domains are not observed at the interface between the NW and Si. The interface is presumably elastic thus preventing threading dislocations from forming.

In order to study the composition dependent height saturation phenomenon of $In_xGa_{1-x}As$ NW array,[15] $In_xGa_{1-x}As$ NW array growth was carried out using a two-step scheme by switching to a higher In composition in the middle of the growth. For comparison, $In_xGa_{1-x}As$ NWs were grown in one step for 20 min with In molar ratio [TMIn/(TMIn+TMGa)] of 0.2, as shown in Figure 3a. The maximum height of the NWs is ∼3 μm, and further growth increases the width but does not increase the NW height. For the two-step scheme, $In_xGa_{1-x}As$ NWs are first grown for 10 min only with In molar ratio of 0.2 (step I), followed by an additional 10-min growth with increased In molar ratio of 0.65 (step II). The side and 45° tilted SEM images of the two-step grown NWs are shown in Figure 3b,c, respectively. It is apparent that two-step growth produces a new set of NWs with a thinner diameter among the thicker NWs, but the maximum height of the thick NWs does not increase noticeably compared with the NWs shown in Figure 3a. This indicates that the crystallization at the NW tip via adatom diffusion is insignificant for the catalyst-free $In_xGa_{1-x}As$ NWs, and the nucleation mostly takes place at the Si−$In_xGa_{1-x}As$ heterointerface instead of the $In_xGa_{1-x}As$−$In_yGa_{1-y}As$ NW heterointerface. This may present challenges to produce axial heterojunction nanowires using this method.

The composition uniformity of the $In_xGa_{1-x}As$ NW has been investigated by EDX analysis. Figure 4b shows the In composition taken from marked points along the NW axis (Figure 4a) for a 3.4 μm long $In_xGa_{1-x}As$ NW. The average In composition is 0.89 ± 0.06, similar to the X-ray diffraction results of the same NW sample.[15] It is interesting to note that the In composition in high In-content $In_xGa_{1-x}As$ NWs (i.e., x > 0.65) is higher than the corresponding In molar ratio in the gas phase, while that of the low In-content $In_xGa_{1-x}As$ (i.e., x < 0.3) NWs is almost the same as the nominal In molar ratio.[15] This phenomenon, in contrast to In incorporation rate in strained $In_xGa_{1-x}As$ thin film growth,[20] is not clearly understood at this point and is a subject for future investigation.

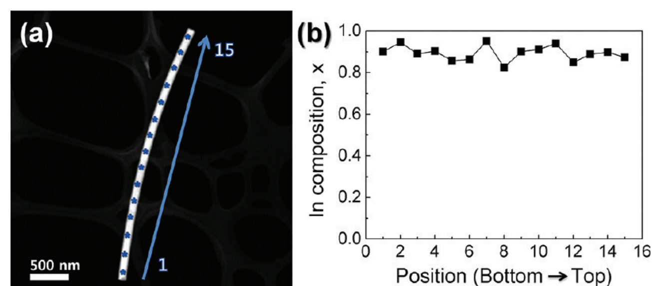

Figure 4. (a) Low-resolution TEM image of a NW indicates the locations where EDX has been analyzed. (b) In composition at the specific points marked in panel a. The In composition is calculated from atomic % of the EDX spectra.

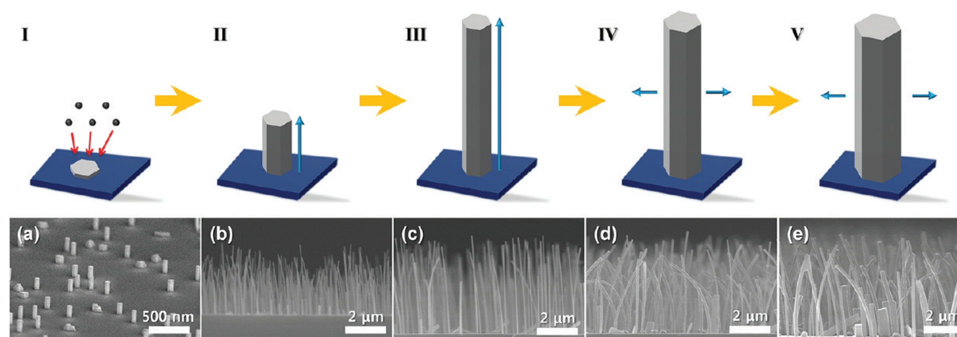

Figure 5. Illustration of the strain-induced $In_xGa_{1-x}As$ NW growth mechanism and corresponding SEM images. (I) The NWs are nucleated on a Si(111) substrate; (II) NWs are grown along the (111) direction; (III) Height of NWs reaches the saturationpoint; (IV, V) The diameter of NWs increases significantly and bending occurs. The corresponding SEM image at each stage is shown in panels a−e.

It is well-known that crystallization from adatom surface diffusion leads to composition variation along vertical ternary $In_xGa_{1-x}As$ NWs due to the mobility difference between In and Ga on the growth substrate. For example, the In composition of a tapered $In_xGa_{1-x}As$ NW grown via VLS varies by as much as 40% along the NW height.[12] As shown in Figure 4b, the composition does not vary much along the NW in our experiments. More importantly, the composition fluctuation is random, in contrast to the VLS growth mode. This indicates that the mechanism of strain-induced $In_xGa_{1-x}As$ NW growth is probably different from that of metal-catalyzed, including self-caralyzed, VLS growth.

Based on all the observations and characterization, the growth evolution for strain-induced $In_xGa_{1-x}As$ NWs is illustrated, along with SEM images at each growth stage, in Figure 5. The strain energy arising from lattice mismatch between $In_xGa_{1-x}As$ and Si is a key factor to initiate catalyst-free, one-dimensional epitaxy. In severely lattice-mismatched systems, the strain energy of the adlayer can be lowered by forming isolated islands via strain-induced island growth or Volmer−Weber mode (stage I).[21] If the diameter of the island is small enough, this system is elastically strained with a fully coherent interface. At this stage, the lateral growth is nearly restricted because the heterointerface is coherent and the formation of misfit dislocation by increasing diameter is not energetically favored.[22] As a result, the islands are preferentially propagated in the ⟨111⟩ direction because of the lowest surface energy in that direction for zinc-blende structured NWs (stage II).[23] As the NW grows, however, the interface gradually becomes inelastic and finally loses its 1-D nature. As a result, the height of $In_xGa_{1-x}As$ NWs is saturated at a certain point (stage III). Once the 1-D growth reaches the saturation point, lateral growth becomes noticeable along with an increase of the curvature of the NWs (stages IV and V). The saturation height of $In_xGa_{1-x}As$ NWs increases with In composition and is inversely proportional to the NW diameter. As shown in Figure S1 of Supporting Information, $In_xGa_{1-x}As$ NWs with 0.65 In molar ratio have diameters less than 100 nm, and the NW height saturates around 7 μm, while $In_xGa_{1-x}As$ NWs with 0.2 In molar ratio have an average diameters of ∼200 nm and do not grow beyond 4 μm in height. Growth conditions, including V/III ratio, change the NW diameter as well as the saturation height. As shown in Figure S2 of Supporting Information, increasing the V/III ratio from 26 to 40 results in an increase of diameter from 200 to 280 nm for the $In_xGa_{1-x}As$ NWs with 0.2 In molar ratio, and a corresponding decrease of the maximum height from ∼4 μm to below 3 μm. These results imply that the height of the NWs may be determined by the interfacial strain energy between the NW and Si, which changes depending on the size of the NW.

■ CONCLUSIONS

The structural characteristics and growth mechanism of strain-induced $In_xGa_{1-x}As$ NWs have been studied. Sharp heterogeneous interface between $In_xGa_{1-x}As$ NWs and Si has been confirmed by cross-sectional TEM analysis. No threading dislocation is found at the interface even though enormous lattice-mismatch strain between $In_xGa_{1-x}As$ and Si exists. In contrast to NWs produced via metal-catalyzed VLS growth mode, strain-induced $In_xGa_{1-x}As$ NWs show a lack of diameter or composition variation along the axial direction, and composition-dependent height saturation. The physical understanding of the growth process reported here provides insight to the growth of bandgap-engineered $In_xGa_{1-x}As$ NW array for applications in advanced optoelectronic devices, as well as monolithic tandem solar cells on Si platform.

■ ASSOCIATED CONTENT

Ⓢ Supporting Information

SEM images for the $In_xGa_{1-x}As$ NW array with varying In molar ratio and varying V/III ratio. This material is available free of charge via the Internet at http://pubs.acs.org.

■ AUTHOR INFORMATION

Corresponding Author

*K.J. Choi: tel, +82-52-217-2337; fax, +82-52-217-2408; e-mail, choi@unist.ac.kr. X. Li: tel, 1-217-265 6354; fax, 1-217-244 6375; e-mail, xiuling@illinois.edu.

Notes

The authors declare no competing financial interest.

■ ACKNOWLEDGMENTS

Financial support was provided in part by NSF STC under Award Number 0749028 (C.M.M.I.) and NSF DMR under Award Number 1006581. Also this research was supported in part by Future-based Technology Development Program (Nano Fields, Grant Number 2010-0029300) and the Converging Research Center Program (Grant Number 2011K000589) through the National Research Foundation of Korea (NRF) funded by the Ministry of Education, Science and Technology.

■ REFERENCES

(1) Capasso, F.; Cho, A. Y. Bandgap engineering of semiconductor heterostructures by molecular beam epitaxy: Physics and applications. *Surf. Sci.* **1994**, *299*−*300*, 878−891.

(2) Nahory, R. E.; Pollack, M. A.; Johnston, W. D.; Barns, R. L. Band gap versus composition and demonstration of Vegard's law for $In_{1-x}Ga_xAs_yP_{1-y}$ lattice matched to InP. *Appl. Phys. Lett.* **1978**, *33* (7), 659−661.

(3) Choi, K. J.; Biegalski, M.; Li, Y. L.; Sharan, A.; Schubert, J.; Uecker, R.; Reiche, P.; Chen, Y. B.; Pan, X. Q.; Gopalan, V.; Chen, L. Q.; Schlom, D. G.; Eom, C. B. Enhancement of ferroelectricity in strained $BaTiO_3$ thin films. *Science* **2004**, *306* (5698), 1005−1009.

(4) Choi, K. J.; Baek, S. H.; Jang, H. W.; Belenky, L. J.; Lyubchenko, M.; Eom, C.-B. Phase-transition temperatures of strained single-crystal $SrRuO_3$ thin films. *Adv. Mater.* **2010**, *22* (6), 759−762.

(5) Kaya, M.; Atici, Y. Studies of lattice mismatch and threading dislocations in GaAs/Si grown by MBE. *Superlattices Microstruct.* **2004**, *35* (1−2), 35−44.

(6) Fitzgerald, E. A. The effect of substrate growth area on misfit and threading dislocation densities in mismatched heterostructures. *J. Vac. Sci. Technol. B* **1989**, *7* (4), 782−788.

(7) Chuang, L. C.; Moewe, M.; Ng, K. W.; Tran, T.-T. D.; Crankshaw, S.; Chen, R.; Ko, W. S.; Chang-Hasnain, C. GaAs nanoneedles grown on sapphire. *Appl. Phys. Express* **2011**, *98* (12), No. 123101.

(8) Hou, W.-C.; Chen, L.-Y.; Tang, W.-C.; Hong, F. C. N. Control of seed detachment in Au-assisted GaN nanowire growths. *Cryst. Growth Des.* **2011**, *11* (4), 990−994.

(9) Tomioka, K.; Tanaka, T.; Hara, S.; Hiruma, K.; Fukui, T. III-V nanowires on Si substrate: Selective-area growth and device applications. *IEEE J. Quantum Electron.* **2011**, *17* (4), 1112−1129.

(10) Sato, T.; Kobayashi, Y.; Motohisa, J.; Hara, S.; Fukui, T. SA-MOVPE of InGaAs nanowires and their compositions studied by micro-PL measurement. *J. Cryst. Growth* **2008**, *310* (23), 5111−5113.

(11) Heun, S.; Radha, B.; Ercolani, D.; Kulkarni, G. U.; Rossi, F.; Grillo, V.; Salviati, G.; Beltram, F.; Sorba, L. Pd-assisted growth of InAs nanowires. *Cryst. Growth Des.* **2010**, *10* (9), 4197−4202.

(12) Kim, Y.; Joyce, H. J.; Gao, Q.; Tan, H. H.; Jagadish, C.; Paladugu, M.; Zou, J.; Suvorova, A. A. Influence of nanowire density on the shape and optical properties of ternary InGaAs nanowires. *Nano Lett.* **2006**, *6* (4), 599−604.

(13) Kang, J.-H.; Gao, Q.; Joyce, H. J.; Tan, H. H.; Jagadish, C.; Kim, Y.; Guo, Y.; Xu, H.; Zou, J.; Fickenscher, M. A.; Smith, L. M.; Jackson, H. E.; Yarrison-Rice, J. M. Defect-free GaAs/AlGaAs core−shell nanowires on Si substrates. *Cryst. Growth Des.* **2011**, *11* (7), 3109−3114.

(14) Allen, J. E.; Hemesath, E. R.; Perea, D. E.; Lensch-Falk, J. L.; LiZ., Y; Yin, F.; Gass, M. H.; Wang, P.; Bleloch, A. L.; Palmer, R. E.; Lauhon, L. J. High-resolution detection of Au catalyst atoms in Si nanowires. *Nat. Nanotechnol.* **2008**, *3* (3), 168−173.

(15) Shin, J. C.; Kim, K. H.; Yu, K. J.; Hu, H.; Yin, L.; Ning, C.-Z.; Rogers, J. A.; Zuo, J.-M.; Li, X. $In_xGa_{1-x}As$ nanowires on silicon: One-dimensional heterogeneous epitaxy, bandgap engineering, and photovoltaics. *Nano Lett.* **2011**, *11* (11), 4831−4838.

(16) Wei, W.; Bao, X.-Y.; Soci, C.; Ding, Y.; Wang, Z.-L.; Wang, D. Direct heteroepitaxy of vertical inas nanowires on Si substrates for broad band photovoltaics and photodetection. *Nano Lett.* **2009**, *9* (8), 2926−2934.

(17) Heiss, M.; Ketterer, B.; Uccelli, E.; Morante, J. R.; Arbiol, J.; Morral, A. F. i. In(Ga)As quantum dot formation on group-III assisted catalyst-free InGaAs nanowires. *Nanotechnology* **2011**, *22* (19), No. 195601.

(18) Zuo, J. M.; Gao, M.; Tao, J.; Li, B. Q.; Twesten, R.; Petrov, I. Coherent nano-area electron diffraction. *Microsc. Res. Tech.* **2004**, *64* (5−6), 347−355.

(19) Chuang, L. C.; Moewe, M.; Chase, C.; Kobayashi, N. P.; Chang-Hasnain, C.; Crankshaw, S. Critical diameter for III-V nanowires grown on lattice-mismatched substrates. *Appl. Phys. Lett.* **2007**, *90* (4), No. 043115.

(20) Lutgen, S.; Marschner, T.; Stolz, W.; Göbe, E. O.; Tapfer, L. Atomic incorporation efficiencies for strained (GaIn)AsGa(PAs) superlattice structures grown by metalorganic vapour phase epitaxy. *J. Cryst. Growth* **1995**, *152*, 1−13.

(21) Eaglesham, D. J.; Cerullo, M. Dislocation-free Stranski-Krastanow growth of Ge on Si(100). *Phys. Rev. Lett.* **1990**, *64* (16), 1943.

(22) Ertekin, E.; Greaney, P. A.; Chrzan, D. C.; Sands, T. D. Equilibrium limits of coherency in strained nanowire heterostructures. *J. Appl. Phys.* **2005**, *97* (11), No. 114325.

(23) Fortuna, S. A.; Li, X. Metal-catalyzed semiconductor nanowires: A review on the control of growth directions. *Semicond. Sci. Technol.* **2010**, *25* (2), No. 024005.